ELSEVIER

Earth and Planetary Science Letters 198 (2002) 417–427

EPSL

www.elsevier.com/locate/epsl

Predicting shear viscosity during volcanic processes at the glass transition: a calorimetric calibration

Joachim Gottsmann [a,b,*], Daniele Giordano [a], Donald B. Dingwell [a]

[a] *Institute for Mineralogy, Petrology and Geochemistry, Theresienstraße 41/III, University of Munich, D-80333 Munich, Germany*
[b] *Department of Earth Sciences, The Open University, Walton Hall, Milton Keynes MK7 6AA, UK*

Received 24 January 2002; accepted 8 February 2002

Abstract

The viscosity of volcanic melts at the glass transition has been determined for 11 compositions ranging from basanite to rhyolite. Determination of the temperature dependence of viscosity, together with the cooling rate dependence of the glass transition, permits the calibration of the value of the viscosity at the glass transition at a given cooling rate for each melt. Temperature-dependent viscosities have been obtained using micropenetration methods in the range 10^8–10^{12} Pa s. Glass transition temperatures have been obtained using differential scanning calorimetry. For each investigated melt composition, the activation energies yielded by calorimetry and viscometry are identical. This confirms that a simple shift factor can be used for each in order to determine the viscosity at the glass transition for a given cooling rate in nature. The results of this study indicate that there is a subtle but significant compositional dependence of the shift factor of a factor of 10 (in log terms) from 10.8 to 9.8. The composition dependence of the shift factor is cast here in terms of a compositional parameter, the mol% of excess oxides (defined within). Using such a parameterisation we obtain a non-linear dependence of the shift factor upon composition that matches the 17 observed values within error. The resulting model permits the prediction of viscosity at the glass transition, during the cooling of glassy volcanic rocks to within 0.1 log units.

Keywords: viscosity; enthalpy; relaxation; magmas; lava; volcanism; eruptions; phase transitions

1. Introduction

The shear viscosity is a primary control on the morphology and textures of volcanic deposits and flows. Viscosity itself is dependent on parameters such as chemical composition and water content [1–4], crystal and/or bubble content [5–8] and, for the case of non-Newtonian flow, stress [9]. Recently, it has been recognised that the liquid–glass transition can play a central role in volcanic eruptions [10]. Intersection of this kinetic boundary, the liquid to glass or so-called 'glass transition', during eruption, can have catastrophic consequences. This is because the mechanical response of the magma or lava to an applied stress at this brittle/ductile transition governs the eruptive behaviour [11] and has hence direct consequences for the assessment of hazards extant during volcanic crises. Whether an applied stress is accom-

* Corresponding author. Tel.: +44-1908-65-97-76; Fax: +44-1908-65-51-51.
E-mail address: j.gottsmann@open.ac.uk (J. Gottsmann).

0012-821X/02/$ – see front matter
PII: S0012-821X(02)00522-8

modated by viscous deformation or by elastic response depends on the timescale of the perturbation with respect to the timescale of the structural response, i.e. the structural relaxation time [12,13]. Viscous response may accommodate very high strains but sustained stress applied to magmas at the glass transition leads to their non-Newtonian behaviour [9] and terminates in the brittle failure of the magma.

The viscosity of the geomaterial at low crystal and/or bubble content is controlled by the viscosity of the melt phase. Knowledge of the melt viscosity enables calculation of the relaxation time τ of the system via the Maxwell relationship:

$$\tau = \frac{\eta_N}{G_\infty} \quad (1)$$

where G_∞ is the shear modulus with a value of $\log_{10}$ (Pa) = 10 ± 0.5 [14] and η_N is the Newtonian shear viscosity. Due to the thermally activated nature of structural relaxation, Newtonian viscosities at the glass transition vary with cooling history. For cooling rates in the order of several K/min, viscosities of approximately 10^{12} Pa s [15] are obtained corresponding to typical relaxation times in the order of 100 s.

Cooling rate data for volcanic glasses across the glass transition have revealed variations of up to seven orders of magnitude from tens of Kelvins per second to less than 1 K per day [16–18]. A logical consequence is that the viscosities at the temperatures where the glass transition occurs will vary substantially. Rapid cooling of a melt will lead to higher glass transition temperatures at lower melt viscosities, whereas slow cooling will have the opposite effect, generating lower glass transition temperatures at correspondingly higher melt viscosities. Indeed, such a quantitative link between viscosities at the glass transition and cooling rate data for obsidian rhyolites based on the equivalence of their enthalpy and shear stress relaxation times has been provided [19]. A similar relation for synthetic melts had been proposed earlier by [20].

Combining calorimetric with shear viscosity data from degassed melts, this study investigates whether the above-mentioned equivalence of relaxation times is valid for a wide range of silicate melt compositions relevant for volcanic eruptions. The result of the comparison is a quantitative link for the prediction of viscosity at the glass transition for melt compositions ranging from ultrabasic to felsic.

2. Methods

2.1. Sample selection

The chemical composition and a description of the samples selected for this study are provided in Table 1. Samples include basanite, trachybasalt, phonotephrite, tephriphonolite, phonolite, trachyte, dacite and rhyolite. All but three rock specimens from which the investigated samples were prepared were sampled by the authors in the field. The compositions are graphically displayed in a total alkali vs. silica diagram (Fig. 1; after [21]).

2.2. Sample preparation

In order to obtain crystal- and bubble-free glasses for viscometry and calorimetry, most samples investigated during this study were melted and quenched. Their compositions hence correspond to virtually anhydrous melts with water contents below 200 ppm, with the exception of samples P3RR and R839. P3RR is a degassed obsidian sample from an obsidian flow with a minor water content of 0.16 wt% (Table 1). The microlite content is less than 1 vol% [25]. The hyaloclastite fragment R839-5.8 has a water content of 0.08 wt% (C. Seaman, personal communication) and a minor microlite content.

Fusing of the samples was performed in thin-walled platinum crucibles in a $MoSi_2$ box furnace at 1 atm and 1300–1600°C (depending on the composition). The samples were transferred to a viscometry furnace where they were fused for several hours until inspection of a stirring spindle inserted into the melts indicated that they were crystal- and bubble-free. The melts were removed from the furnace and allowed to quench in air. Diamond cored right cylinders from the glasses with a diameter of approximately 6 mm were

Table 1
Chemical composition and description of the investigated samples

Location	Sample	Composition	SiO_2	TiO_2	Al_2O_3	FeO	MnO	MgO	CaO	Na_2O	K_2O	P_2O_5	H_2O	Total	e.o. (mol%)	Sample origin
	EIF	Basanite	41.22	2.74	12.12	10.13	–	11.26	15.69	2.76	3.05	1.02	–	99.82	30.18	Synthetic composition; obtained from C. Shaw
Etna (I)	ETN	Trachybasalt	47.81	1.94	17.91	10.90	0.19	4.75	9.96	3.94	2.11	0.48	–	99.42	12.22	1992 lava flow; collected by M. Coltelli [4]
Vesuvius	Ves_g	Phonotephrite	49.71	0.84	16.57	7.27	0.13	5.15	10.31	2.73	6.57	0.73	–	98.99	16.91	Vesuvius 1631 eruption; [22]
Vesuvius (I)	Ves_w	Tephriphonolite	51.95	0.68	18.87	6.19	0.13	2.54	7.41	3.81	8.02	0.41	–	99.00	10.26	Vesuvius 1631 eruption; [22]
Hawaii (USA)	R839-5.8[a]	Basalt	52.11	2.61	13.69	11.06	0.16	6.37	11.00	2.33	0.41	0.25	0.08	99.73	14.35	Hyaloclastite fragment; provided by C. Seaman
Astroni (I)	ATN	Phonolite	60.63	0.49	18.02	3.24	0.19	0.58	2.57	5.06	9.15	0.07	–	99.80	3.63	Tephra from the Astroni 3.8 ka BP eruption; [23]
Montana Blanca (E)	MB5	Phonolite	60.68	0.56	18.88	3.32	0.20	0.36	0.68	9.79	5.47	0.06	–	99.64	2.23	Obsidian flow from Tenerife; [24]
Montana Blanca (E)	MB5-6.61[b]	Phonolite	60.40	0.56	18.81	3.53	0.21	0.34	0.65	9.82	5.54	0.13	0.08	99.75	1.59	–
Monte Nuovo (I)	MNV	Trachyte	64.57	0.31	17.29	2.93	0.13	0.24	1.84	5.74	6.90	0.05	–	98.93	3.24	1538 Monte Nuovo eruption
Povoação (P)	PVC	Trachyte	65.27	0.45	17.30	2.60	0.14	0.32	0.85	6.46	6.52	0.09	–	99.02	4.01	Povoação ignimbrite (Azores)
Unzen (J)	UZN	Dacite	66.58	0.37	15.37	4.11	0.10	2.23	5.06	3.87	2.18	0.14	–	99.13	5.03	1993 dome eruption
Lipari (I)	P3RR	Rhyolite	75.37	0.07	12.84	1.57	0.07	0.04	0.72	4.19	5.13	–	0.14	99.43	1.15	Obsidian flow from Lipari; [25]
Armenia	EDF[c]	Rhyolite	77.18	0.09	12.91	0.61	0.07	0.07	0.51	4.05	4.52	0.01	0.10	100.05	0.15	–
Little Glass Butte (USA)	LGB[c]	Rhyolite	77.45	0.06	12.96	0.71	0.03	0.05	0.53	4.05	4.17	–	–	100.32	0.41	–
Ben Lomond (NZ)	BL6[c]	Rhyolite	77.99	0.17	12.25	1.22	0.04	0.17	1.08	3.66	3.39	0.03	0.17	99.57	0.20	–
Eburru (EAK)	KE5[c]	Pantellerite	72.50	0.28	8.23	7.57	0.24	0.01	0.29	6.57	4.30	–	0.21	98.98	3.82	–
Mayor Island (NZ)	8 ka[c]	Pantellerite	73.74	0.23	9.57	5.58	0.13	0.01	0.22	5.94	4.27	0.03	0.16	99.21	5.60	–

[a] Analysis provided by C. Seaman (Caltech, USA; personal communication).
[b] Data from [24].
[c] Data from [19].
Samples were analysed by microprobe; oxides are calculated volatile-free and normalised to 100 wt%. FeO = analysed as bulk iron; totals expressed as original analytical totals. Water contents where given were analysed by FTIR. Microprobe was operated at 15 kV acceleration voltage (10 nA) and a peak count time of 20 s (background 10 s) using a defocused 20 μm wide beam. Calibration is based on mineral standards. e.o. (mol%): excess oxides are calculated by subtracting the sum of the molar percentages of Al_2O_3, TiO_2 and 0.5FeO (regarded as structural network formers) from the sum of the molar percentages of oxides regarded as network modifying (0.5FeO, MnO, MgO, CaO, Na_2O, K_2O, P_2O_5, H_2O) [27,29–32].

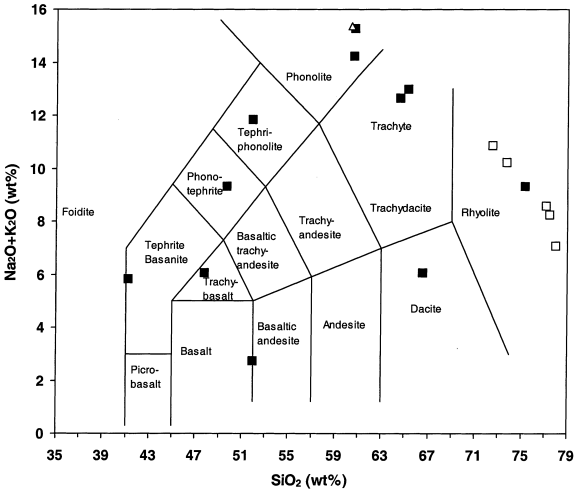

Fig. 1. Total alkali vs. silica diagram (after [21]) of the investigated compositions. Filled squares are data from this study, open squares and open triangle represent data from [19,24], respectively.

cut into 2–3 mm thick disks, polished dried and kept in a desiccator until their use in both viscometry and calorimetry.

Glass compositions of melted and natural samples were analysed by electron microprobe. Results are presented in Table 1. Sample MB5 stems from the same sequence from which sample MB5-3.61 of [24] was collected. Close inspection of both chemical data sets reveals that fusing and dehydration have no effect on major element chemistry (Table 1).

2.3. Micropenetration viscometry

Micropenetration techniques [26] were applied to determine melt viscosities in the range 10^8–10^{12} Pa s [27]. The method involves determining the rate at which a hemispherical Ir indenter under a fixed load progresses into the melt surface. The measurements were performed using a Baehr® DIL 802 V pushrod dilatometer in vertical geometry under a constant argon flow. The shear viscosity η can be calculated via:

$$\eta = \frac{0.1875\mathrm{Pt}}{r^{0.5}\alpha^{1.5}} \quad (2)$$

([26], and references therein). r is the radius of the half-sphere, P the applied force, α is the indent distance and t is time ($t=0$, $\alpha=0$ upon application of the force). Viscosities determined on the NBS (NIST) standard SRM 711 have been reproduced within an error of ± 0.06 log units.

The samples were heated in the viscometer at a constant heating rate of 10 K/min to a temperature of approximately 170 K below the measurement temperature. Subsequently heated at a rate of 5 K/min to the target temperature, the samples were allowed to structurally relax during a 60 min isothermal dwell, before the indenter was lowered to penetrate the sample.

In comparison to the study by [19] potential vesiculation occurring during our viscosity measurements had not to be taken into account because (i) our investigated bulk compositions were anhydrous (also no indication of vesiculation in the natural glass samples) and (ii) viscometry was performed at generally higher viscosities. Within our operating window of less than 70 min at the respective temperatures (Table 2) vesiculation did not occur in our samples. In addition, no indication of crystallisation during the course of the viscosity measurements was observed. Our data correspond to viscosity values for the melt phase (Table 2).

2.4. Differential scanning calorimetry

Samples on which viscometry had been performed were subsequently used in the calorimeter. The differential scanning calorimeter (Netzsch® DSC 404 Pegasus) was calibrated against the specific heat capacity at constant pressure (c_p) of a single crystal sapphire. The temperature calibration was performed using melting temperatures of standard materials (In, Sn, Bi, Zn, Al, Ag and Au). The glass sample disks were placed in Pt/Rh crucibles and heated in order to measure their specific heat capacities as a function of temperature. A thermal procedure including rate heating across the glass transition into the supercooled liquid field and subsequent rate cooling was applied as follows. First heating of the samples was performed at 5 K/min approximately 50 K above their glass transition temperature to allow complete structural relaxation. Through a set of sub-

Table 2
Viscometry and differential scanning calorimetry results

Sample	Viscometry			Calorimetry			
	T (°C)	$10\,000/T$ (K^{-1})	$\log_{10}\eta$ (Pa s)	q (K/min)	$\log_{10}q$ (K/s)	T_g (°C)	$10\,000/T_g$ (K^{-1})
EIF	680	10.49	11.41	5	−1.08	695	10.33
	692	10.36	10.77	10	−0.78	699	10.28
	702	10.25	10.26	20	−0.48	706	10.21
	710	10.17	9.94				
	740	9.87	8.69				
ETN	673	10.57	11.65	5	−1.08	712	10.15
	731	9.96	10.23	10	−0.78	722	10.05
	747	9.80	9.94	15	−0.60	729	9.98
				20	−0.48	735	9.92
R839-5.8	678	10.51	10.47	5	−1.08	663	10.68
	689	10.39	10.00	8	−0.88	669	10.62
	696	10.32	9.68	10	−0.78	672	10.58
	712	10.15	9.14	16	−0.57	678	10.51
	731	9.96	8.73	20	−0.48	681	10.48
Ves_w	705	10.22	10.66	5	−1.08	700	10.28
	724	10.03	10.15	10	−0.78	712	10.15
	743	9.84	9.85	20	−0.48	723	10.04
Ves_g	729	9.98	9.78	5	−1.08	691	10.38
	745	9.82	9.51	10	−0.78	699	10.28
	756	9.71	9.13	20	−0.48	712	10.15
	767	9.61	8.79				
PVC	723	10.04	10.77	5	−1.08	696	10.32
	739	9.88	10.41	10	−0.78	707	10.20
	750	9.78	10.19	20	−0.48	721	10.06
	761	9.67	9.95				
	782	9.48	9.63				
MNV	696	10.32	11.32	5	−1.08	699	10.29
	744	9.83	10.83	10	−0.78	708	10.19
	757	9.71	10.71	20	−0.48	721	10.06
	795	9.36	10.36				
ATN	761	9.67	10.30	5	−1.08	708	10.19
	775	9.55	10.11	10	−0.78	723	10.04
	794	9.37	9.73	20	−0.48	735	9.92
	831	9.06	9.11				
MB5	615	11.26	11.63	5	−1.08	634	11.03
	651	10.82	10.85	8	−0.88	640	10.95
	673	10.57	10.32	10	−0.78	643	10.91
	692	10.37	10.00	16	−0.57	654	10.79
	737	9.90	8.99	20	−0.48	659	10.72
UZN	774	9.55	9.90	5	−1.08	722	10.05
	801	9.31	9.28	10	−0.78	732	9.95
	818	9.16	8.91	20	−0.48	744	9.83
P3RR	720	10.06	11.10	5	−1.08	713	10.14
	738	9.89	10.78	8	−0.88	722	10.05
	770	9.59	10.18	10	−0.78	730	9.97
	811	9.23	9.56	16	−0.57	742	9.85
	841	8.98	9.15	20	−0.48	746	9.81

sequent thermal treatments at which the heating rates matched the previous cooling rates of 20, 16, 10, 8 and 5 K/min, the glass transition temperatures were set in relation to the experimentally applied cooling rates (Fig. 2; see below). Note that the glass transition temperature during this study is taken as the peak value of the heat capacity curve. Glass transition temperatures were determined to within ± 2 K.

3. Results and discussion

3.1. Viscometry

Table 2 lists the results for the viscosity measurements using micropenetration techniques. The viscosity-inverse temperature data are fitted via a linear expression, which results in an Arrhenian dependence of viscosity with temperature (Fig. 3). This approximation is regarded to be valid over the restricted temperature and viscosity range covered by micropenetration viscometry. It is however worth emphasising that the entire viscosity–temperature relationship from liquidus temperatures to temperatures close to the glass transition for many of the investigated melts may be regarded as non-Arrhenian. This discussion is given elsewhere [27].

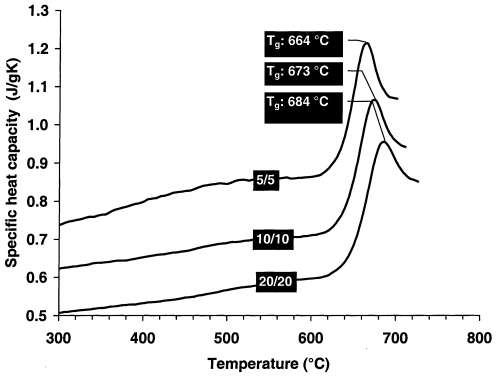

Fig. 2. The specific heat capacity as a function of temperature for the investigated basalt sample (R839-5.8). The curves represent c_p traces obtained during reheating the sample in the calorimeter to record the respective glass transition temperature as a function of cooling rate. With matching heating and cooling rates of 20, 10, and 5 K/min such derived glass transition temperatures differ about 20 K. The quantification of the shift in glass transition temperatures (taken as the peak of the c_p curve) as a function of cooling rate enables to calculate the activation energy for enthalpic relaxation (Table 2). The curves are displaced along the y-axis for clarity.

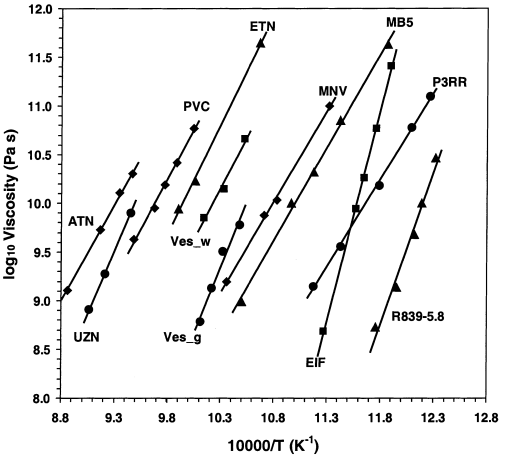

Fig. 3. The viscosities obtained for the investigated samples using micropenetration viscometry. The data (Table 2) are fitted by an Arrhenian expression (Eq. 3). Resulting parameters are given in Table 3. Viscosity data are shifted along the x-axis for clarity.

Employing an Arrhenian fit:

$$\log_{10}\eta = \log_{10}A_\eta + \frac{E_\eta}{2.303RT} \quad (3)$$

to our viscosity–temperature data results in the determination of the activation energy for viscous flow (shear stress relaxation) E_η and a pre-exponential factor A_η. R is the universal gas constant (J/mol K) and T is the temperature in K.

Activation energies for viscous flow vary between 349 kJ/mol for rhyolite and 845 kJ/mol for basanite. The higher activation energies at low temperatures of the basic compositions may be explained by their more drastic viscosity increase with decreasing temperature, as opposed to those for felsic compositions. This reflects the pronounced non-Arrhenian viscosity–temperature relationship of the basic liquids over their entire magmatic temperature range [27].

3.2. Differential scanning calorimetry

The glass transition temperatures (T_g) derived

Table 3
Comparison of parameters derived from viscometry and differential scanning calorimetry

Composition	Sample	Viscosity measurements		DSC measurements		Shift factor
		$\log_{10}A_\eta$	E_η (kJ/mol)	$\log_{10}A_{DSC}$	E_{DSC} (kJ/mol)	
Basanite	EIF	−34.4 ± 0.2	845 ± 70	−51.1 ± 0.1	915 ± 68	9.64 ± 0.08
Trachybasalt	ETN	−20.3 ± 0.1	516 ± 42	−25.3 ± 0.1	524 ± 28	9.72 ± 0.08
Basalt	R839-5.8	−22.9 ± 0.1	613 ± 38	−30.8 ± 0.1	577 ± 38	9.81 ± 0.07
Phonotephrite	Ves_g	−17.6 ± 0.1	533 ± 35	−26.9 ± 0.3	514 ± 33	9.80 ± 0.07
Tephriphonolite	Ves_w	−10.9 ± 0.0	488 ± 29	−24.6 ± 0.1	484 ± 34	9.84 ± 0.06
Trachyte	PVC	−10.8 ± 0.1	417 ± 19	−21.4 ± 0.2	421 ± 87	10.17 ± 0.08
Trachyte	MNV	−7.1 ± 0.1	387 ± 30	−25.6 ± 0.2	422 ± 39	10.14 ± 0.08
Phonolite	ATN	−8.3 ± 0.1	390 ± 31	−21.5 ± 0.2	417 ± 48	10.18 ± 0.10
Phonolite	MB5-6.61[a]	−9.8 ± 0.2	365 ± 38	−20.3 ± 0.2	372 ± 37	10.03 ± 0.08
Phonolite	MB5	−10.0 ± 0.1	373 ± 28	−21.2 ± 0.2	380 ± 32	10.16 ± 0.08
Dacite	UZN	−15.6 ± 0.1	490 ± 33	−25.1 ± 0.1	518 ± 26	10.10 ± 0.09
Rhyolite	P3RR	−7.0 ± 1.2	349 ± 23	−16.7 ± 0.1	338 ± 21	10.24 ± 0.08
Rhyolite	BL6[b]	−8.6 ± 0.1	389 ± 14	−19.5 ± 0.1	391 ± 33	10.80 ± 0.16
Rhyolite	EDF[b]	−7.1 ± 0.1	374 ± 22	−18.6 ± 0.1	396 ± 25	10.39 ± 0.16
Rhyolite	LGB[b]	−7.9 ± 0.1	387 ± 8	−19.8 ± 0.1	412 ± 14	10.61 ± 0.15
Pantellerite	8 ka[b]	−8.8 ± 0.1	327 ± 12	−18.7 ± 0.1	322 ± 31	10.21 ± 0.16
Pantellerite	KE5[b]	−8.6 ± 0.1	297 ± 8	−17.9 ± 0.1	287 ± 10	10.07 ± 0.16

[a] Data from [24].
[b] Data from [19].

from the heat capacity data obtained during the thermal procedures described above may be set in relation to the applied cooling rates (q). An Arrhenian fit to our q vs. $1/T_g$ data in the form of:

$$\log_{10}|q| = \log_{10}A_{DSC} + \frac{E_{DSC}}{2.303RT_g} \quad (4)$$

gives the activation energy for enthalpic relaxation E_{DSC} and the pre-exponential factor A_{DSC}. R is the universal gas constant and T_g is the glass transition temperature in K. The fits to the q vs. $1/T_g$ data are graphically displayed in Fig. 4. The activation energies derived for enthalpic relaxation vary between 338 and 915 kJ/mol of rhyolite and basanite, respectively. They thus show a similar range as the activation energies found for viscous flow. Data are reported in Table 3.

3.3. The equivalence of enthalpy versus shear stress relaxation times

Activation energies for both shear stress and enthalpy relaxation are within error equivalent for all investigated compositions (Table 3). Based on the equivalence of the activation energies we propose the equivalence of enthalpy and shear stress relaxation times for a wide range of degassed silicate melts relevant during volcanic eruptions (Fig. 5). For a number of synthetic

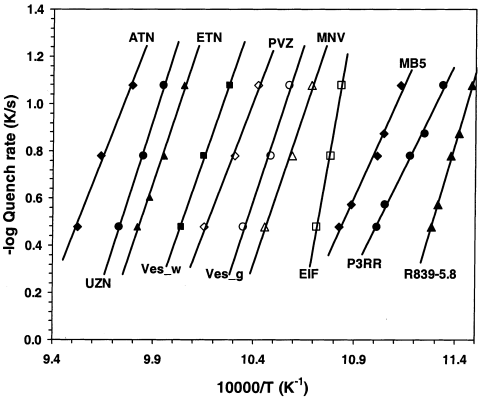

Fig. 4. The glass transition temperatures T_g as a function of quench rates obtained for the investigated compositions. Data were recorded using a differential scanning calorimeter. The quench rate vs. $1/T_g$ data (cf. Table 2) are fitted by an Arrhenian expression given in Eq. 4. The resulting parameters are shown in Table 3. Data sets are displaced along the x-axis for clarity.

melts and for rhyolitic obsidians a similar equivalence was suggested earlier by [19,20,28], respectively. The data presented by [19] are directly comparable to our data and are therefore included in Table 3 as both studies involve (i) dry or degassed silicate melt compositions and (ii) a mutually consistent definition and determination of the glass transition temperature. The equivalence of both enthalpic and shear stress relaxation times implies the applicability of a simple algorithm (Eq. 5) to combine both shear viscosity and cooling rate data to predict the viscosity at the glass transition using a constant shift factor K ([19,20]):

$$\log_{10}\eta(\text{at } T_g) = K - \log_{10}|q| \quad (5)$$

To a first approximation, this relation appears to be independent of the chemical composition. However, below we will see that the shift factor may indeed be further refined in terms of a composition dependence.

Eq. 5 allows the determination of the individual shift factors for the compositions investigated. These constants are also reported in Table 3 together with those of the study from [19]. The constant K found by [20] to satisfy Eq. 5 was 11.4. The average shift factor for rhyolitic melts determined by [19] was 10.65 ± 0.28. The average shift factor for our investigated compositions is 9.99 ± 0.16. The reason for the mismatch of the shift factor determined by [19] with the shift factor proposed by [20] lies in the different definitions of the glass transition temperature. Correcting the data to match the definition of T_g employed during our study and the study by [19] results in mutually consistent data. A detailed description and analysis of the correction procedure is given in [19] and is not repeated here. Close inspection of our shift factor data permits the identification of a compositional dependence (Table 3). The value of K varies from 9.64 for the most basic melt composition to 10.24 (Fig. 6, Table 2) for our investigated calc-alkaline rhyolite P3RR. [19] postulated in their study a dependence of K for rhyolites as a function of the agpaitic index.

Fig. 6 displays the shift factors now available for natural silicate melts (including those determined by [19]) as a function of excess oxides expressed in mol%. Calculating excess oxides as opposed to the agpaitic index helps us to better constrain the effect of the chemical composition on the melt structure, such as small variations in the alkali and water content of the individual samples. As mentioned above, it is the structural relaxation time that defines the glass transition. Excess oxides are calculated by subtracting the sum of the molar percentages of Al_2O_3, TiO_2 and 0.5FeO (regarded as structural network formers) from the sum of the molar percentages of oxides regarded as network modifying (0.5FeO, MnO, MgO, CaO, Na_2O, K_2O, P_2O_5, H_2O) [27,29–32]. One half of the molar FeO content is considered as network modifying, the other as network forming. There appears to be a log natural dependence of the shift factors with excess oxides in the melt structure. Knowledge of the

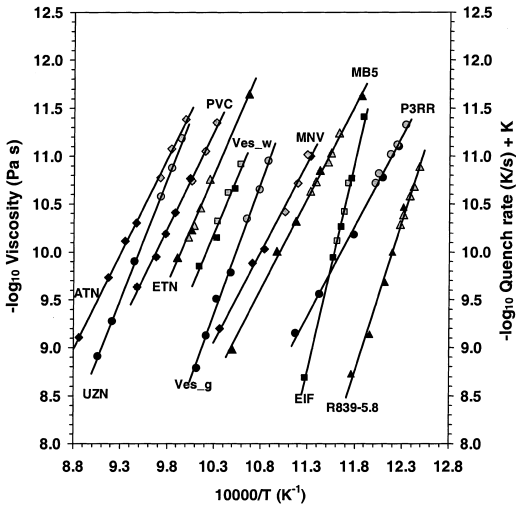

Fig. 5. The equivalence of the activation energies of enthalpy and shear stress relaxation in silicate melts. Both quench rate vs. $1/T_g$ data and viscosity data are related via a shift factor K to predict the viscosity at the glass transition. The individual shift factors are given in Table 3. Black symbols represent viscosity vs. inverse temperature data, grey symbols represent cooling rate vs. inverse T_g data to which the shift factors have been added. The individually combined data sets are fitted by a linear expression to illustrate the equivalence of the relaxation times behind both thermodynamic properties. Data sets are displaced along the x-axis for clarity.

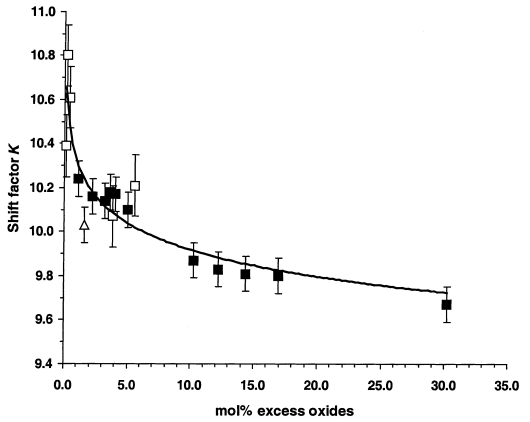

Fig. 6. The shift factors as a function of the molar percentage of excess oxides of the investigated compositions. Filled squares are data from this study, open squares represent data calculated from [19]. The open triangle indicates the composition published in [24]. There appears to be a log natural dependence of the shift factors as a function of excess oxides in the melt composition (see Eq. 6). Knowledge of the shift factor allows predicting the viscosity at the glass transition for a wide range of degassed or anhydrous silicate melts relevant for volcanic eruptions via Eq. 5.

molar amount of excess oxides thus enables the determination of the shift factor via:

$$K = 10.321 - 0.175 \times \ln x \quad (6)$$

$$(R^2 = 0.824)$$

where x is the molar percentage of excess oxides.

3.4. Implications for the rheology of volcanic processes

Knowledge of the viscosity at the glass transition is a vital contribution for the modelling of volcanic processes. Depending on the timescale of a perturbation a viscoelastic silicate melt can experience the glass transition at viscosities that may range over more than 10 orders of magnitude [33]. The rheological properties of the matrix melt in a multiphase system (melt+bubbles+crystals) will determine whether the system will be driven out of structural equilibrium and will consequently cross the glass transition upon an applied stress. For situations where cooling rate data are available our results permit estimation of the viscosity at which the magma crossed the glass transition and evolved from a viscous (ductile) to a brittle system. This transition is the essential phenomenon ending magmatic behaviour via fragmentation during explosive volcanism or the cessation of the flow of lava.

If natural glass is present in volcanic rocks then the cooling process may be quantified partially by directly analysing the structural state of the glass. The glassy phase contains a structural memory, which can reveal the kinetics of cooling across the glass transition [34]. Such a geospeedometer has been applied recently to several volcanic facies [16–18,24,25,35]. That work has shown that vitrification during volcanism can be the consequence of cooling at rates that vary by up to seven orders of magnitude. For example, cooling rates across the glass transition are reported for evolved compositions from 10 K/s for tack-welded phonolitic spatter [17] to less than 10^{-5} K/s for pantellerite obsidian flows involving thermal annealing [16,25]. Applying the corresponding shift factors allows proposing that viscosities associated with their vitrification may have differed as much as six orders of magnitude from $\log_{10}$ 9.0 Pa s to $\log_{10}$ 15.2 Pa s (calculated from Eq. 4). For basic composition, such as basaltic hyaloclastite fragments, available cooling rate data across the glass transition [18,36] between 2 K/s and 0.0025 K/s would indicate that the associated viscosities were in the range of $\log_{10}$ 9.4–12.3 Pa s.

The structural relaxation times (calculated via Eq. 1) associated with the viscosities at the glass transition vary over six orders of magnitude for the observed cooling rates. This implies that for the fastest cooling events it would have taken the structure only 0.1 s to re-equilibrate in order to avoid the transition, yet, apparently the thermal perturbation of the system was on an even faster timescale. For the slowly cooled pantellerite flows in contrast, structural relaxation may have taken more than 1 day to be achieved. A detailed discussion about the significance of very slow cooling rates and the quantification of the structural response of supercooled liquids during annealing is given in [35].

The glass transition is associated with a drastic change of the derivative thermodynamic properties such as expansivity and heat capacity. It is

also the rheological limit of viscous deformation of lava. The modelling of volcanic processes must therefore involve the accurate determination of this transition [13].

Most lavas are liquid-based suspensions containing crystals and bubbles. The rheological description of such systems remains experimentally challenging (see [37] for a review). A partial resolution of this challenge is provided by the shift factors presented here (as demonstrated by [19]). The quantification of the melt viscosity should enable to better constrain the influence of both bubbles and crystals on the bulk viscosity of a variety of silicate melt compositions.

4. Conclusions

The combination of calorimetric and viscometric data yields a simple compositionally dependent algorithm for the prediction of the shear viscosity at the glass transition for multicomponent liquids ranging from basanite to rhyolite. The basis for this is the equivalence of the relaxation times for enthalpy and shear stress relaxation for the wide range of silicate melt compositions demonstrated during this study. Nevertheless, the shift factor that relates cooling rate data with viscosity at the glass transition appears to be slightly dependent on the melt composition. Due to the equivalence of relaxation times of the thermodynamic properties viscosity, enthalpy and volume [33,38] knowledge of the glass transition is generally applicable to the assignment of liquid versus glassy values of magma properties for the simulation and modelling of volcanic eruptions. It is however worth mentioning that the available shift factors should only be employed to predict viscosities at the glass transition for degassed silicate melts. It remains an experimental challenge to achieve proposing an equivalent relationship between viscosity and cooling rate data [39] for hydrous silicate melts.

Acknowledgements

This work was funded by grants to D.B.D. from the Deutsche Forschungsgemeinschaft (Di 431) and the European Union (ENV4-CT97-0713). J.G. was additionally supported by the EU Research and Training Network 'Volcano Dynamics' (HPRN-CT-2000-00060). The authors thank C. Shaw, C. Seaman and M. Coltelli for providing samples. The manuscript benefited from constructive reviews from M.C. Wilding and an anonymous reviewer.*[AC]*

References

[1] K.-U. Hess, D.B. Dingwell, Viscosities of hydrous leucogranitic melts: A non-Arrhenian model, Am. Mineral. 81 (1996) 1297–1300.
[2] D.B. Dingwell, K.-U. Hess, C. Romano, Extremely fluid behaviour of hydrous peralkaline rhyolites, Earth Planet. Sci. Lett. 158 (1998) 31–38.
[3] D. Giordano, D.B. Dingwell, C. Romano, Viscosities of Teide phonolites in the welding interval, J. Volcanol. Geotherm. Res. 103 (2000) 239–245.
[4] D. Giordano, D.B. Dingwell, Viscosity of hydrous Etna basalt: implications to the modeling of Plinian basaltic eruptions, Bull. Volcanol. (2002) in press.
[5] D.B. Dingwell, N.S. Bagdassarov, G.Y. Bussod, S.L. Webb, Magma rheology, in: Handbook on Experiments at High Pressure and Applications to the Earth's Mantle, M.A.o. Canada, 21 edn., 1993, pp. 1–42.
[6] N.S. Bagdassarov, D.B. Dingwell, Frequency dependent rheology of vesicular rhyolite, J. Geophys. Res. 98 (1993) 6477–6487.
[7] M. Manga, J. Castro, K.V. Cashman, M. Loewenberg, Rheology of bubble-bearing magmas, J. Volcanol. Geotherm. Res. 87 (1998) 15–28.
[8] A.M. Lejeune, Y. Bottinga, T.W. Trull, P. Richet, Rheology of bubble-bearing magmas, Earth Planet. Sci. Lett. 166 (1999) 71–84.
[9] S.L. Webb, D.B. Dingwell, Non-Newtonian rheology of igneous melts at high stresses and strain rates: experimental results for rhyolite, andesite, basalt, and nephelinite, J. Geophys. Res. 95 (1990) 15695–15701.
[10] D.B. Dingwell, Volcanic dilemma: flow or blow?, Science 273 (1996) 1054–1055.
[11] H. Sato, T. Fugii, S. Nakada, Crumbling of dacite dome lava and generation of pyroclastic flows at Unzen volcano, Nature 360 (1992) 664–666.
[12] C.T. Moynihan, Structural relaxation and the glass transition, in: J.F. Stebbins, P.F. McMillan, D.B. Dingwell (Eds.), Structure, Dynamics and Properties of Silicate Melts, Vol. 32, Reviews in Mineralogy, Mineralogical Society of America, Washington, DC, 1995, pp. 1–19.
[13] D.B. Dingwell, Relaxation in silicate melts: some applications, in: J.F. Stebbins, P.W. McMillan, D.B. Dingwell (Eds.), Structure, Dynamics and Properties of Silicate

Melts, Vol. 32, Reviews in Mineralogy Mineralogical Society of America, Washington, DC, 1995, pp. 21–66.
[14] D.B. Dingwell, S.L. Webb, Relaxation in silicate melts, Eur. J. Mineral. 2 (1990) 427–449.
[15] H. Scholze, N.J. Kreidl, Technological aspects of viscosity, in: D.R. Uhlmann, N.J. Kreidl (Eds.), Glass. Science and Technology, Vol. 3, Academic Press, London, 1986, pp. 233–273.
[16] M.C. Wilding, S.L. Webb, D.B. Dingwell, Evaluation of a relaxation geospeedometer for volcanic glasses, Chem. Geol. 125 (1995) 137–148.
[17] M. Wilding, S.L. Webb, D.B. Dingwell, G. Ablay, J. Marti, Cooling variation in natural volcanic glasses from Tenerife, Canary Islands, Contrib. Mineral. Petrol. 125 (1996) 151–160.
[18] M. Wilding, D.B. Dingwell, R. Batiza, L. Wilson, Cooling rates of hyaloclastites: applications of relaxation geospeedometry to undersea volcanic deposits, Bull. Volcanol. 61 (2000) 527–536.
[19] R.J. Stevenson, D.B. Dingwell, S.L. Webb, N.S. Bagdassarov, The equivalence of enthalpy and shear stress relaxation in rhyolitic obsidians and quantification of the liquid–glass transition in volcanic processes, J. Volcanol. Geotherm. Res. 68 (1995) 297–306.
[20] G.W. Scherer, Use of the Adam–Gibbs equation in the analysis of structural relaxation, J. Am. Ceram. Soc. 67 (1984) 504–511.
[21] M.J. LeBas, R.W. LeMaitre, A. Streckeisen, B. Zanetti, A chemical classification of volcanic rocks based on the total alkali-silica diagram, J. Petrol. 27 (1986) 745–750.
[22] M. Rosi, C. Principe, R. Vecci, The Vesuvius 1631 eruption. A reconstruction based on historical and stratigraphical data, J. Volcanol. Geotherm. Res. 58 (1993) 151–182.
[23] M.M. Di Vito, R. Isaia, G. Orsi, J. Southon, S. de Vita, M. D'Antonio, L. Pappalardo, M. Piochi, Volcanism and deformation since 12 000 years at the Campi Flegrei caldera (Italy), J. Volcanol. Geotherm. Res. 91 (1999) 221–246.
[24] J. Gottsmann, D.B. Dingwell, Cooling dynamics of spatter-fed phonolite obsidian flows on Tenerife, Canary Islands, J. Volcanol. Geotherm. Res. 105 (2001) 323–342.
[25] J. Gottsmann, D.B. Dingwell, The cooling of frontal flow ramps: A calorimetric study on the Rocche Rosse rhyolite flow, Lipari, Aeolian Islands, Italy, Terra Nova 13 (2001) 157–164.
[26] K.-U. Hess, D.B. Dingwell, S.L. Webb, The influence of excess alkalis on the viscosity of a haplogranitic melt, Am. Mineral. 80 (1995) 297–304.
[27] D. Giordano, D.B. Dingwell, Towards a multicomponent model for the non-Arrhenian temperature-dependence of viscosity for anhydrous melts, Earth Planet. Sci. Lett. (2002) submitted.
[28] O.S. Narayanaswamy, Thermorheological simplicity in the glass transition, J. Am. Ceram. Soc. 71 (1988) 900–904.
[29] D.B. Dingwell, R. Knoche, S.L. Webb, The effect of P_2O_5 on the viscosity of haplogranitic liquid, Eur. J. Mineral. 5 (1993) 133–140.
[30] M.J. Toplis, D.B. Dingwell, The variable influence of P_2O_5 on the viscosity of melts of differing alkali/aluminium ratio: Implications for the structural role of phosphorus in silicate melts, Geochim. Cosmochim. Acta 60 (1996) 4107–4121.
[31] E.A.K. Middlemost, Iron oxidation ratios, norms and the classification of volcanic rocks, Chem. Geol. 77 (1989) 19–26.
[32] B.O. Mysen, The Structure and Properties of Silicate Melts, Elsevier, Amsterdam, 1988, 354 pp.
[33] S.L. Webb, Shear, volume, enthalpy and structural relaxation in silicate melts, Chem. Geol. 96 (1992) 449–457.
[34] M.A. DeBolt, A.J. Easteal, P.B. Macedo, C.T. Moynihan, Analysis of structural relaxation in glass using rate heating data, J. Am. Ceram. Soc. 59 (1976) 16–21.
[35] J. Gottsmann, D. Dingwell, The thermal history of a spatter-fed lava flow: The 8-ka pantellerite flow on Mayor Island, New Zealand, Bull. Volcanol. (2002) in press.
[36] J. Gottsmann, D.B. Dingwell, The cooling history of submarine vitrophyres: a preliminary calorimetric study on drill cores of the HSDP, EOS 81 (2000) 1348.
[37] D.B. Dingwell, Recent experimental progress in the physical description of magma relevant to explosive volcanism, in: J.S. Gilbert and R.S.J. Sparks (Eds.), The Physics of Explosive Eruptions, Vol. 145, Special Publications, Geological Society, London, 1998, pp. 9–26.
[38] S.L. Webb, R. Knoche, D.B. Dingwell, Determination of silicate liquid thermal expansivities using dilatometry and calorimetry, Eur. J. Mineral. 4 (1992) 95–104.
[39] Y. Zhang, J. Jenkins, Z. Xu, Kinetics of the reaction $H_2O+O=2$ OH in rhyolitic glasses upon cooling: Geospeedometry and comparison with glass transition, Geochim. Cosmochim. Acta 61 (1997) 2167–2173.